Dynamics of a Supercooled Ionic Liquid Studied by Optical and Dielectric Spectroscopy

Naoki Ito, Wei Huang, and Ranko Richert*

Department of Chemistry and Biochemistry, Arizona State University, Tempe, Arizona 85287-1604

Received: November 30, 2005; In Final Form: January 10, 2006

We have measured the dynamics of solvation of a triplet state probe, quinoxaline, in the glass-forming ionic liquid dibutylammonium formate near its glass transition temperature $T_g = 153$ K. The Stokes-shift correlation function displays a relaxation time dispersion of considerable magnitude and the optical line width changes systematically along the solvation coordinate. The solvent dynamics in the viscous regime is compared with the rotational behavior of the solute and with the dielectric relaxation of the ionic liquid. Among the different quantities derived from the dielectric experiments, the relaxation of the macroscopic electric field, i.e., the modulus $M(t)$, matches best the solvent response $C(t)$ regarding time scale and stretching exponent. Many other properties are reminiscent of the behavior of polar molecular liquids which lack the ionic character.

1. Introduction

Ionic liquids have unique properties, such as low vapor pressure, thermal stability, and high electric conductivity, which make them versatile alternatives to conventional and often toxic and volatile organic solvents in many applications.[1−6] By designing and combining ionic species it could be possible to customize the properties for particular applications. To further assess the potential of these "green" solvents, molecular aspects of ionic liquids have been studied. For example, several spectroscopic methods are used to examine the dynamics of ionic liquids: optical Kerr effect,[7−10] vibrational,[11] electron spin,[12−14] and nuclear magnetic resonance spectroscopy.[15−18] Computer simulations also have been utilized to understand dynamics of ionic liquids on a molecular scale.[19−23]

Solvation in ionic liquids has been a subject of numerous studies regarding basic properties such as polarity and dynamics. Several investigations have focused on the solvating property of ionic liquids and compared with that of conventional organic liquids. Static "polarity" based on solvatochromic shift of electronic excitations for selected dye probes shows values comparable to those of linear alcohols.[24−27] As for the dynamics of solvation,[28] solvent response times in different ionic liquids have been measured by using various fluorescence probes.[29−39] Compared with typical room temperature solvents, slower solvation times as a result of higher viscosities appear to be common features of solvation dynamics in ionic liquids studied to date. Additionally, the relaxation behavior is generally more nonexponential or dispersive relative to isoviscous molecular liquids.

It is well established that some of the ionic liquids retain their liquid nature when cooled below their melting points, i.e., these liquids become supercooled and eventually reach the glassy state with further cooling.[40,41] It has been suggested that the flexible alkyl-chain of some cations creates the potential energy surface that is essential to glass forming materials.[42,43] Generally, the dynamics of supercooled liquids shows two prominent features: nonexponentiality of the responses and non-Arrhenius behavior of the temperature dependence.[44] Angell et al. have investigated dynamic properties such as viscosity of some ionic liquids at their supercooled liquid states.[45−47] It will be interesting to see how the nonexponential character of solvation dynamics observed already at room temperature evolves as ionic liquids are supercooled and eventually form ionic glasses.

In this study we examine the dynamics of a supercooled ionic liquid, dibutylammonium formate (DBAF). This compound belongs to a class of proton-transfer ionic liquids, which are promising media for electrochemical applications.[45−50] Solvation dynamics and probe rotation data in the viscous state are obtained by using quinoxaline as a triplet-state probe and studying the time-resolved emission spectra of the $T_1 \rightarrow S_0(0-0)$ transition.[51,52] Dielectric relaxation measurements are also performed, which provide complementary information on the relaxation behavior of the macroscopic dipole moment and of the electric field. Only a few studies on dielectric relaxations of ionic liquids are available, e.g., ethylammonium nitrate[53] and some imidazolium ionic liquids.[54−56] In contrast to these cases, we observe that dc and ac conductivities of DBAF are well separated in time. It is found that solvation dynamics is as nonexponential near T_g as many other ionic liquids at room temperature. The solvation time scales match those of the electric modulus $M = 1/\epsilon$, which corresponds to the relaxation time of the macroscopic electric field.

2. Experimental Section

Dibutylammonium formate (DBAF) was obtained from the lab of C. A. Angell and dried under vacuum at 40 °C for several hours before use. Quinoxaline (QX) was purified by sublimation before use. For the solvation and probe rotation measurements, samples were prepared by dissolving the solute QX in the solvent DBAF at a concentration of around 10^{-4} mol/mol.

The sample cell for optical measurements is a stainless steel frame holding two quartz windows that are vacuum-sealed by Kalrez O-rings. The cell is mounted to the cold stage of a closed cycle He refrigerator (Leybold, RDK 10-320, RW 3) and temperature stability within ±30 mK is achieved by a temperature controller (Lake Shore, LS 330) equipped with calibrated diode sensors (Lake Shore, DT-470-CU-13). Temperature gradients near the sample are greatly reduced (<0.5 K) by an aluminum shield that guides radiation heat to the first cooling stage at ∼80 K.

Solvation and probe rotation are studied by measuring the time dependent phosphorescence of the probe QX. Two different

10.1021/jp056960v CCC: $33.50
Published on Web 02/11/2006

excitation light sources are used: an excimer laser (GAM Laser, EXC-200/100) operated at $\lambda_{exc} = 308$ nm with pulse width ≈25 ns and a frequency tripled Nd:YAG laser (Continuum, SLI-10) operated at $\lambda_{exc} = 355$ nm with pulse width ≈6 ns. The repetition rate is adjusted such that the pulses are separated by at least three times the phosphorescence lifetime τ_{ph} of the QX molecule, typically 0.5 Hz. The output of the excimer laser is polarized vertically ($\alpha = 0°$, normal to the plane defined by the laser, sample, and detector), using a Glan-Taylor polarizer, while that of the Nd:YAG laser is already polarized. Variable polarization angles $\kappa = 0°...90°$ of the excitation are achieved by $\lambda/2$ quartz retardation plates, designed for the respective laser wavelength, $\lambda_{exc} = 308$ or 355 nm. The retardation plate is positioned under computer control by a rotation stage (Newport, ESP-300, PR50CC). The optics are adjusted such that the incident intensity remains practically independent of the angle κ. All cryostat and sample cell windows are UV grade synthetic fused silica with extremely low luminescence and birefringence. The excitation beam size is limited to ensure that no depolarized reflection from the cell frame or cryostat reenters the sample. The phosphorescence emission is polarized by a Glan-Thompson polarizer set to an angle $\beta = 0°$ and UV is removed from the detection path with use of a UV cutoff filter. As a result of having the detector angle fixed at zero, the viewing angle of the setup and the detector's angular sensitivity become irrelevant.

For spectrally resolved experiments, the phosphorescence emission is dispersed by a triple grating polychromator (Acton Research, SpectraPro-275) and registered by a MCP intensified diode array camera (EG&G, 1455B-700-HQ) with controller (EG&G, 1471A), gating options (EG&G, 1304), and synchronization facilities (SRS, DG-535). The spectra consist of 730 channels with a resolution of 0.12 nm/channel for the 600 g/mm blazed grating. The system is wavelength calibrated with Xe and Kr lamps. Across the typical redshifts of ∼300 cm^{-1} the spectral sensitivity is sufficiently flat so that uncorrected emission data are used. The time resolution is defined by gating the camera with gate delays between 1 μs and 1 s, and the gate width typically being set to ≤10% of the delay time. Spectra are recorded by accumulating the signals from typically 900 excitation pulses. To obtain anisotropy spectra, the emission is recorded with a resolution of 0.12 nm for the three polarization angles $\kappa = 0°$, 54.7°, and 90°. The time-resolved solvation dynamics experiments all refer to the $T_1 \rightarrow S_0(0-0)$ emission of the probe QX, measured at the magic angle $\kappa = 54.7°$. The values of anisotropy are obtained from the amplitudes of Gaussian fits to polarized spectra ($\kappa = 0°$ and 90°) to obtain high signal sensitivity.

The dielectric measurements of DBAF are conducted by holding the liquid sample between two stainless steel disk electrodes (20 mm ∅) which are separated by Teflon strips with a thickness of 50 μm arranged in a radial geometry. Frequency dependent impedance measurements are performed in the range 0.1 Hz ≤ f ≤ 10 MHz, using a Solartron SI-1260 gain-phase analyzer, equipped with a Mestec DM-1360 transimpedance amplifier as described previously.[57] The empty sample capacitor is employed as a reference for the impedance measurements. All samples are measured inside a nitrogen-gas cryostat where the temperature is stabilized and measured by a Novocontrol Quatro controller. The cooling rate of ≈10 K/min turns out to suppress the crystallization of the sample.

3. Results and Discussion

3.1. Phosphorescence Characteristics. Phosphorescence spectra of QX in glassy DBAF at 148 K ($T_g = 156$ K determined by differential scanning calorimetry[58]) are shown in Figure 1. The two emission spectra obtained for the polarization angles $\kappa = 0°$ (I_{VV}) and 90° (I_{VH}) are used to calculate an anisotropy spectrum according to

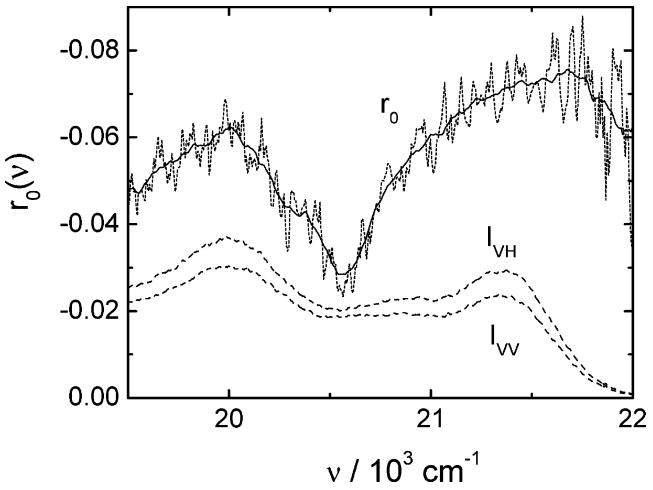

Figure 1. Phosphorescence $I(\nu)$ and anisotropy spectra $r_0(\nu)$ of quinoxaline (QX) in glassy dibutylammonium formate (DBAF) at 148 K. The polarized emission spectra (dashed lines) are recorded at a delay time of 10 ms and a gate time of 10 ms, identified as I_{VV} for $\kappa = 0°$ and I_{VH} for $\kappa = 90°$. The anisotropy is shown as raw data and as a smoothed curve (25 point adjacent average).

$$r(\nu,t) = \frac{I_{VV}(\nu,t) - I_{VH}(\nu,t)}{I_{VV}(\nu,t) + 2I_{VH}(\nu,t)} = r_0(\nu)g_2(t) \qquad (1)$$

Here and in the following, we will use "ν" for the wavenumber (instead of frequency). In eq 1, $r_0(\nu)$ is the wavenumber dependent fundamental anisotropy (determined by the angle between emission and absorption transition dipole) and $g_2(t)$ is the (single particle, rank 2) orientational correlation function of the probe molecule. The value of $r(\nu)$ is negative (ca. −0.1) when QX is excited at $\lambda_{exc} = 308$ nm, while positive (ca. +0.05) if subject to $\lambda_{exc} = 355$ nm excitation, consistent with a fundamental anisotropy $r_0 = -0.13$ (angle $\delta = 70°$) found for QX exited at $\lambda_{exc} = 308$ nm in molecular glass formers.[59−61] Because the data in Figure 1 refer to the glassy state, probe rotation is frozen and there is no relevant time dependence.

Figure 2 shows the temperature dependence of the peak energy for fixed delays and integration times. With increasing temperature, the peak energy shows a redshift between the plateau values of 21 350 and 21 050 cm^{-1} at low and high temperatures, respectively. The total energy shift $\Delta\nu$ between the low- and high-temperature limits is 300 cm^{-1}. The total shift $\Delta\nu$ equals the time-resolved dynamic Stokes shift, because the plateau values at low and high temperature correspond to $\nu_p(t=0)$ and $\nu_p(t\rightarrow\infty)$, respectively. They are the peak energy before and after solvation due to structural rearrangement of the solvent, which is frozen below T_g on the experimental time scale and completed before the delay time at sufficiently high temperature. As a result of the well-developed plateaus, there is no need to consider unresolved solvent responses. Note that the temperature dependence of $\nu_p(0)$ and $\nu_p(\infty)$ is negligible compared to the total shift for the present condition of small temperature variations. A significant fraction of the total redshift is observed between the 1 and 10 ms traces for temperatures between 155 and 165 K. The anisotropy recorded at 10 ms shows a similar behavior but the $r(T)/r_0$ curve in Figure 2 is shifted to higher temperatures relative to the peak energy trace

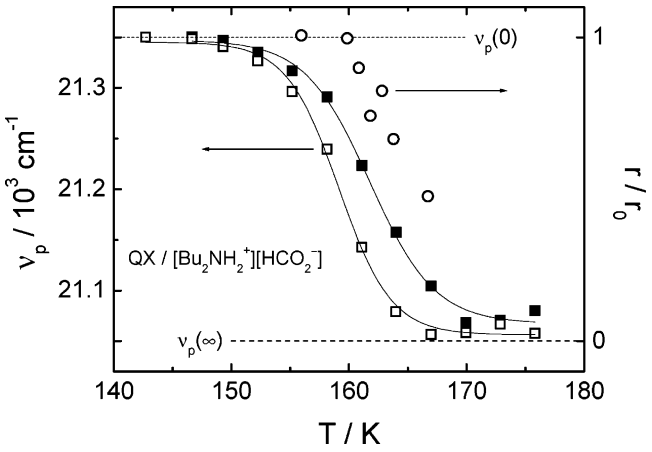

Figure 2. Peak energies ν_p of the $T_1 \rightarrow S_0(0-0)$ band of QX in DBAF at temperatures from 143 to 176 K. Delay and gate times are fixed at 1 (solid squares) and 10 ms (open squares). Open circles denote the results of anisotropy data r/r_0 for 10 ms delay and gate time with the rhs ordinate. The solid lines are guides only. The dashed lines indicate the limiting peak energies $\nu_p(0)$ and $\nu_p(\infty)$ as indicated.

TABLE 1: Solvent and Solute Characteristics of QX in DBAF[a]

solvent	T_g/K	ϵ_s	ϵ_∞	$\nu_p(0)$/cm^{-1}	$\Delta\nu$/cm^{-1}	τ_{ph}/ms
DBAF	153	43	3.5	21350	300	85
3MP	77.5	2.1	2.1	21350	72	265
MTHF	89.4	19	3.0	21290	247	270
NPOH	93.5	81.8	3.0	21302	483	

[a] Data for the molecular glass formers 3-methylpentane (3MP), 2-methyltetrahydrofuran (MTHF), and *n*-propanol (NPOH) are listed for comparison and taken from refs 68 and 69. The lifetime in 3MP is taken from ref 61.

$\nu_p(T)$, which suggests that probe rotation is slower than the dynamics of solvation.

In Table 1 these phosphorescence characteristics are compared with conventional molecular glass formers. It is found that the "polarity" $\Delta\nu$ of the ionic liquid probed with triplet state solvation of QX is moderate and lies between those of 2-methyltetrahydrofuran and *n*-propanol, a moderately polar aprotic and a linear alcohol glass-forming solvent, respectively. As noted earlier, solvatochromic studies on UV−vis absorption and fluorescence in ionic liquids also have observed similar results.[24−27] Therefore, the solvent effect of ionic liquids on probe phosphorescence appears to be very similar to those on other singlet−singlet electronic transitions. The phosphorescence lifetime of QX is substantially smaller in the ionic liquid (less than 100 ms around T_g). The strong temperature dependence of the lifetime near T_g suggests that diffusive motion of a quencher, presumably oxygen, is involved.

3.2. Nonexponential Solvation Dynamics. Figure 3 shows the time-dependent peak energy $\nu_p(t)$ of QX in DBAF at temperatures near T_g. At 146.4 K, the peak energy remains near $\nu_p(0)$ over the present time window of ~1 ms to 1 s. As the temperature is increased by less than 20 K, the behavior changes dramatically. At the highest temperature of 163.1 K, about one-half of the total redshift has occurred within the first 1 ms. This drastic effect of temperature on the dynamics is typical for many glass-forming liquids near T_g, and reflects the pronounced effective activation energy for solvent reorganization in these viscous liquids. At higher temperatures, significant loss of signal intensity prohibits a meaningful data analysis.

The phosphorescence spectra below and above T_g provide reliable estimates of $\nu_p(0)$ and $\nu_p(\infty)$ values, and result in well-

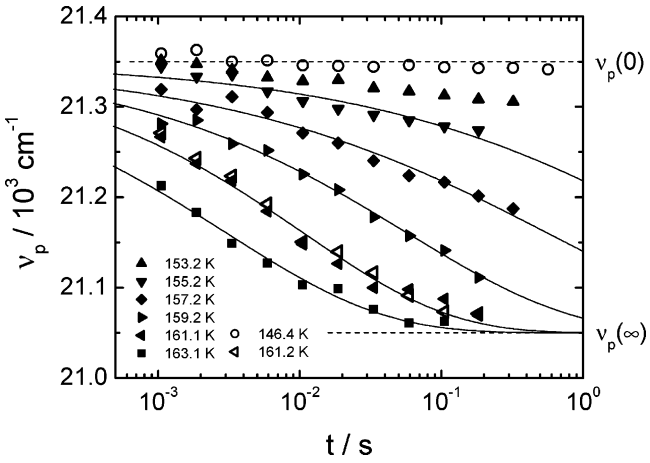

Figure 3. Time-resolved emission peak energies ν_p of the $T_1 \rightarrow S_0$-(0−0) band of QX in DBAF. Different symbols are for different temperatures between 146.4 and 163.1 K as indicated. Open and solid symbols represent two independently prepared samples. The solid lines are KWW fits with the common parameters $\nu_p(0) = 21350$ cm^{-1}, $\Delta\nu = 300$ cm^{-1}, and $\beta_{KWW} = 0.4$ but a different value of τ for each temperature. The dashed lines indicate the limiting peak energies ν_p-(0) and $\nu_p(\infty)$ as indicated.

defined spectral response functions $C(t)$,

$$C(t) = \frac{\nu_p(t) - \nu_p(\infty)}{\nu_p(0) - \nu_p(\infty)} \quad (2)$$

which in other cases was not always simple nor straightforward.[62] The solid lines in Figure 3 are the results of Kohlrausch−Williams−Watts (KWW) fits,

$$C(t) = \exp\left[-\left(\frac{t}{\tau}\right)^{\beta}\right] \quad (3)$$

to $C(t)$ at each temperature, using the values of $\nu_p(0)$ and $\nu_p(\infty)$ from temperature scan measurements as in Figure 1. The value of the KWW exponent for solvation, β_{sol}, decreases somewhat as the temperature decreases when it is fit independently for each temperature, although a constant value of $\beta_{sol} = 0.4$ can reproduce the data for all temperatures reasonably well. That the value of β_{sol} is much smaller than unity implies that the dynamics of solvation deviates considerably from single-exponential behavior.

Many studies on ionic liquid dynamics have found similar deviations from single exponential relaxation, although the extent of the deviation depends on which dynamic is being examined. A recent study has combined subpicosecond with pico- to nanosecond time resolutions and thereby found that solvation time scales are spread over nearly five decades in time.[38] It is interesting to note that very similar values of $\beta_{sol} = 0.4 \pm 0.1$ have been observed for the Stokes shift correlation function $C(t)$ of many ionic liquids with different types of ionic species and for various sample temperatures.[37,38]

A distribution of relaxation times generally leads to a nonexponential relaxation and a stretched exponential (KWW) function has been applied to describe dynamics in many types of supercooled liquids.[44] We use a KWW function here mainly to facilitate a comparison of the ionic liquid and molecular glass formers studied previously by characterizing the dynamics in the same way. While a value of $\beta = 0.4$ is not unusual for a deeply supercooled liquid with relaxation times around 1 s, one expects a significantly larger value of β where the relaxation time is nanoseconds to picoseconds. In contrast to typical

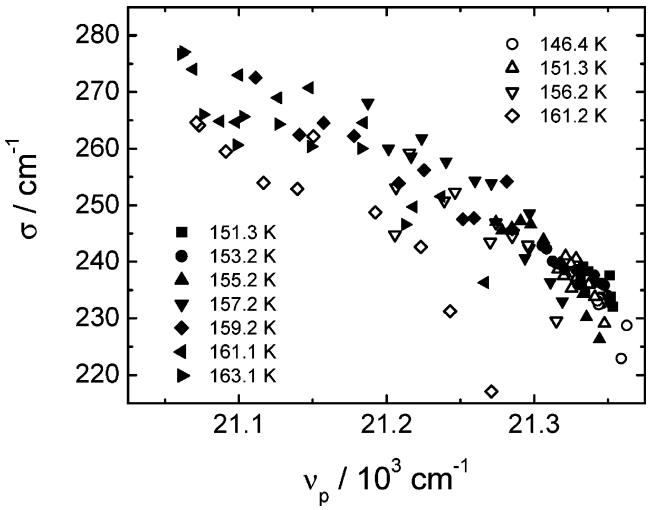

Figure 4. Correlation of inhomogeneous spectral widths σ and peak energies ν_p of time-resolved phosphorescence spectra of QX in DBAF near T_g. Symbols correspond to data obtained for different times between 1 and 680 ms and for temperatures ranging from 146.4 to 163.1 K. Open and solid symbols represent two independently prepared samples.

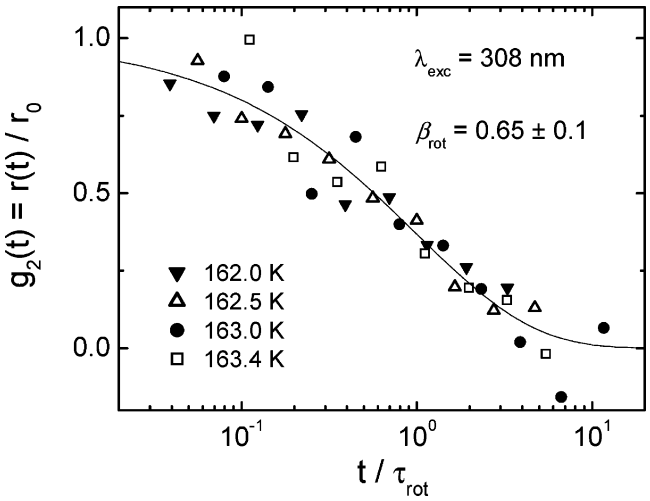

Figure 5. Master plot of probe rotation correlation function $g_2(t)$ vs t/τ_{rot}. Different symbols represent different temperatures as indicated. On the basis of the temperature invariant values of τ_{rot}/τ_{sol}, data for different temperatures are rescaled according to the VFT fit to the solvation time τ_{sol}. The solid line is a KWW function with $\beta_{KWW} = 0.65$.

molecular liquids, we find that the relaxation time dispersion at T_g is similar to the values observed at elevated temperatures and much lower viscosities.

3.3. Spectral Width. The optical emission bands of triplet states at low temperature are well approximated by Gaussian profiles regarding the wavenumber-dependent emission intensity,

$$I(\nu) = I_0 \exp\left[-\frac{(\nu - \nu_p)^2}{2\sigma^2}\right] \quad (4)$$

The inhomogeneous line width σ of optical spectra often provides additional information on the solvent environment around the probe. For example, the time-dependent width observed in 2-methyltetrahydrofuran (MTHF) has been associated with the heterogeneous nature of the solvent response.[63,64] The bandwidths of the emission spectra for QX and Coumarin 153 in MTHF are observed to have a maximum value at intermediate times at a fixed temperature, indicating that probes in fast solvent environments have already relaxed considerably while those in slow environments have hardly changed their emission energy. For the current QX/DBAF system, heterogeneous dynamics is expected to generate a peak in $\sigma(t)$ with a maximum approximately 35 cm^{-1} above the steady-state value of the line width,[65] but no such behavior is observed. It should be noted that heterogeneity regarding the dynamics has not yet been identified experimentally for ionic liquids.

In the present system the width is more strongly correlated with the emission energy than with either time or temperature, as shown in Figure 4. Thus, the effect of heterogeneity could be obscured by a dominant correlation of the energy and width. This correlation suggests that the solvent fluctuations in ionic liquids change systematically along the solvation coordinate and that such a solvation process cannot be described within the framework of linear response theory. On the basis of simulation work, it has been suggested that the effect of polarizability is not negligible in ionic liquids.[18,21] This could be the origin of nonlinear solvation responses, resulting in fluctuations which change along the solvation coordinate.[66]

3.4. Probe Rotation Dynamics. The time window for optical anisotropy measurements is limited by the phosphorescence lifetime of QX, which decreases rapidly with increasing temperature above T_g. On the other hand, the rotation times become very slow as the temperature approaches T_g. These two factors set the limits of the temperature range to a relatively small window in the present system where we can determine rotation times from optical depolarization measurements.

The value of the KWW exponent for probe rotation β_{rot} is determined from a master plot shown in Figure 5. The values of the ratio τ_{rot}/τ_{sol} from the KWW fit to data at each temperature are averaged and utilized to normalize the time axis. Within this narrow temperature window, changes in parameters β, r_0, and τ_{rot}/τ_{sol} should be small compared to uncertainties of the results of each fit. Therefore, a master plot is advantageous for characterizing the probe rotation dynamics. The results are summarized in Table 2 together with concomitant values for other molecular glass formers.

From the data in Figure 5, we derive a ratio of $\tau_{rot}/\tau_{sol} = 6$ and a stretching exponent of $\beta_{rot} = 0.65$. A systematic comparison of probe rotation and solvation dynamics for triplet probes in organic molecular solvents has established a correlation between sizes and dynamics according to $\tau_{rot}/\tau_{sol} = 50 m_{guest}/m_{host} - 40$.[59,60] The present time scale ratio of 6 would correspond to the ratio of $m_{guest}/m_{host} = 0.92$ assuming that the relation established for nonionic glass formers would also hold for QX/DBAF. This calculated mass ratio is comparable to that of QX to cation or ion pair mass, but the value of $\beta_{rot} = 0.65$ exceeding the solvation counterpart $\beta_{sol} = 0.40$ by 0.25 is not consistent with the observations on molecular systems. Probe rotation being significantly more exponential than solvation dynamics required much slower rotation times and time-averaging over fluctuating environments[67] (rate exchange) was made responsible for the diminished effect of heterogeneous dynamics.[59,60] Regarding the present QX/DBAF case, a possible explanation could be that not the entire dispersion of solvent responses is due to dynamic heterogeneity, i.e., that some intrinsic nonexponentiality contributes to β_{sol} being as small as 0.4.

3.5. Dielectric Measurements. Dielectric relaxation experiments provide detailed information on the permittivity and dynamics of polar solvents and thus first steps toward rationalizing the time scale and amplitude of Stokes shift dynamics of dipolar solutes.[28,52] Figure 6 shows the real and imaginary parts

TABLE 2: Comparison of Solvation and Probe Rotation Dynamics for QX in Various Solvents[a]

solvent (host)	m_h/g mol^{-1}	R_m	β_{sol}	β_{rot}	τ_{rot}/τ_{sol}
DBAF	175.3	0.74	0.40 ± 0.05	0.65 ± 0.1	6
dibutylammonium (cation)	130.3	1.00			
formate (anion)	45.0	2.89			
3MP	86.2	1.51	0.5	1.0	50
MTHF	86.1	1.51	0.5	1.0	35
NPOH	60.1	2.17	0.5	0.8	95

[a] The size relations are characterized by the molecular weight of the guest QX (m_g) and of the host (m_h) and by the ratio $R_m = m_g/m_h$. The dynamics parameters are the KWW exponent β_{sol} of the Stokes shift correlation function $C(t)$, KWW exponent β_{rot} of the probe rotation $g_2(t)$, and the ratio of probe rotation (τ_{rot}) and solvation (τ_{sol}) time scales. Data for the molecular solvents 3MP, MTHF, and NPOH are from ref 59.

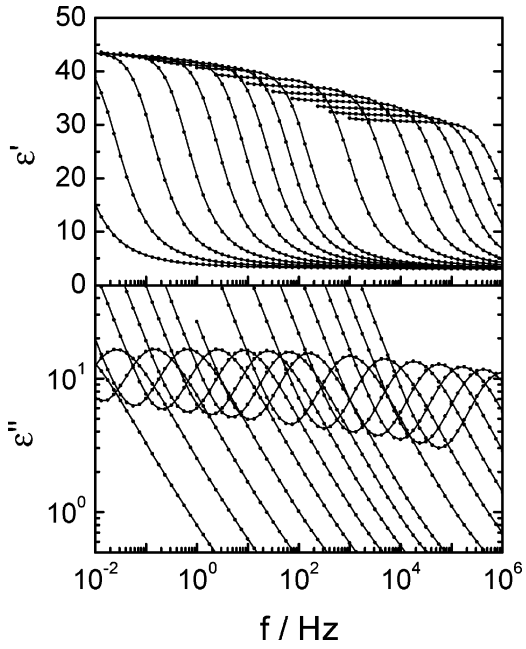

Figure 6. Dielectric permittivity $\epsilon'(\omega)$ (upper panel) and loss $\epsilon''(\omega)$ (lower panel) spectra of viscous DBAF. In the order from low to high transition or peak frequency, the temperatures are 154 to 170 K in steps of 2 K and 175 to 205 K in steps of 5 K. The curves show distinct dc-conductivity and dielectric relaxation contributions.

of the dielectric function $\epsilon^*(\omega)$ of DBAF in the viscous regime above T_g. In contrast to the case of some imidazolium based ionic liquids and ethylammonium nitrate at room temperature,[53,54] the dc-conductivity is sufficiently small such that we can clearly identify a separate α-peak in the $\epsilon''(\omega)$ spectrum. This separation from dc-conductivity from the remaining peak is more reminiscent of dielectric loss curves in molecular glass-forming liquids. To quantify the dielectric behavior as a function of temperature, the dielectric loss curves are fitted by using a Havriliak−Negami (HN) type relaxation function combined with a dc-conductivity term,

$$\epsilon^*(\omega) = \epsilon' - i\epsilon'' = \epsilon_\infty + \frac{\epsilon_s - \epsilon_\infty}{[1 + (i\omega\tau_\epsilon)^\alpha]^\gamma} + \frac{\sigma_{dc}}{i\omega\epsilon_0} \quad (5)$$

Here, ϵ' and ϵ'' are the real and imaginary parts of the dielectric function, while ϵ_s and ϵ_∞ are the low- and high-frequency limits of the dielectric constant, respectively. The value of τ_ϵ characterizes the time scales of the polarization process and the exponents α and γ gauge the broadening and asymmetry of the loss peak. Within the experimental range of Figure 6, 154 to 205 K, α decreases from 0.99 to 0.95 and γ increases from 0.68 to 0.79 upon raising the temperature. The average product is $\langle\alpha\gamma\rangle = 0.72$, which corresponds to a time domain KWW exponent of $\beta_\epsilon \approx 0.8$, indicative of only moderately pronounced

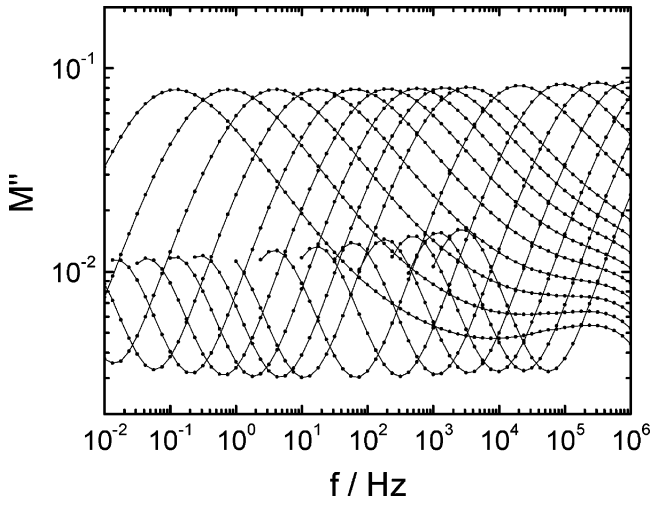

Figure 7. The imaginary part of the dielectric modulus $M''(\omega)$ of DBAF. In the order from low to high transition or peak frequency, the temperatures are 154 to 170 K in steps of 2 K and 175 to 205 K in steps of 5 K. The lower frequency peaks represent dc-conductivity, the larger amplitude peaks correspond to those seen in Figure 6, and additional small secondary peaks appear around $f = 100$ kHz.

deviations from the exponential or Debye case. The high-frequency permittivity ϵ_∞ ($\approx n^2$) is approximately 3.2, while the dielectric relaxation strength $\Delta\epsilon = \epsilon_s - \epsilon_\infty$ drops from 40 to 26 in the 156 to 205 K range, indicative of a substantial polarity as expected.

On the basis of the high dielectric relaxation strength of $\Delta\epsilon = 40$ near T_g, the electric field relaxation or electric modulus

$$M^*(\omega) = \frac{1}{\epsilon^*(\omega)} = M' + iM'' = \frac{M_\infty - M_s}{[1 + (i\omega\tau_M)^\alpha]^\gamma} + \frac{M_s}{1 + i\omega\tau_\sigma} \quad (6)$$

shows a behavior which differs from that of the dielectric retardation $\epsilon^*(\omega)$. The time- or frequency-dependent electric modulus ($M = 1/\epsilon$) quantifies the relaxation of the (macroscopic) electric field at constant charge conditions, and the dc-conductivity (σ_{dc}) turns into a Debye (single time constant, exponential) peak with a time constant $\tau_\sigma = \epsilon_0\epsilon_s/\sigma_{dc}$. The modulus representation of the loss data is shown in Figure 7, again emphasizing the separation of dc- and ac-conductivity by 3.3 decades in time. The characteristic modulus relaxation time τ_M is around 1.1 decades faster than the τ_ϵ values of eq 5. Also, the dispersion of the electric modulus peak is more pronounced than that of the dielectric loss peak, reflected by the smaller value of $\beta_M \approx 0.53$ compared with $\beta_\epsilon \approx 0.8$. Unlike the loss spectra $\epsilon''(\omega)$, the $M''(\omega)$ curves display small secondary peaks at high frequencies.

3.6. Comparison of Optical and Dielectric Measurements. Figure 8 shows an activation plot of relaxation times: solvation and probe rotation from optical measurement of QX in DBAF;

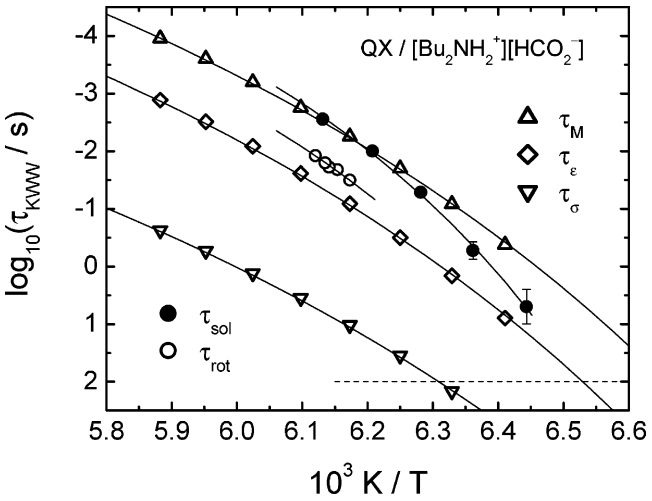

Figure 8. Activation plot of solvation time τ_{sol} (solid circles), probe rotation time τ_{rot} (open circles), electric relaxation time τ_M (triangles up), dielectric retardation time τ_ϵ (diamonds), and conductivity time τ_σ (triangles down) vs inverse temperature for the QX/DBAF system. The solid lines are the VFT fits summarized in Table 3. The dashed line indicated the 100 s criterion for T_g.

TABLE 3: Comparison of Optical and Dielectric Results for the KWW Exponents β and the VFT Fit Parameters of Eq 7[a]

	β_{KWW}	A	B/K	T_0/K	T_g/K	m
τ_{sol}	0.40 ± 0.05	-10.4	206.7	136.6	153.3	114
τ_{rot}	0.65 ± 0.1	-9.63	(206.7)	(136.6)	(154.4)	(101)
τ_ϵ	0.80 ± 0.05	-12.01	443.5	121.5	153.2	68
τ_σ	1.00	-9.49	450.4	119.3	158.5	46
τ_M	0.53 ± 0.05	-13.00	450.3	120.2	150.2	75

[a] Glass transition temperature T_g ($\tau = 100$ s) and fragility index m are obtained from the VFT fits.

permittivity and conductivity from dielectric measurements of DBAF. The temperature dependence of the dynamics is characterized by using Vogel−Fulcher−Tammann (VFT) fits,

$$\log_{10}(\tau/s) = A + B/(T - T_0) \qquad (7)$$

and the results for the adjustable parameters are summarized in Table 3. At higher temperatures the solvation time is the fastest among the correlation times considered, as observed repeatedly in molecular glass formers. As noted earlier, the temperature dependence of probe rotation time appears to follow that of solvation within the limited temperature range. On the other hand, the temperature dependence of the solvent response times, τ_{sol}, is steeper than that of the dielectric retardation, τ_ϵ. This "decoupling" is particularly obvious for times in excess of 200 ms, with only a fraction of the deviation being accounted for by increased uncertainties due to excited-state lifetime limitations. The data with $\tau_{sol} < 100$ ms matche the activation energy and VFT curvature exhibited by all activation traces associated with the dielectric experiments, τ_M, τ_ϵ, and τ_σ, and at elevated temperatures the solvation times approach the values of the modulus τ_M. As seen in Table 3 and Figure 8, the VFT behavior of these latter three time constants differs mainly in their values of A (preexponential factor), implying essentially parallel curves for the dielectric data.

Regarding the comparison of absolute time scales, the solvation times are closest to the dielectric relaxation time τ_M. The other times τ_ϵ and τ_σ are 1.1 and 3.3 decades slower than the modulus time scale, respectively. The dielectric function $\epsilon^*(\omega)$ of the ionic liquid DBAF, see Figure 6, is reminiscent of the signals observed for molecular liquids, where the asymmetric loss peak and conductivity wing originate from dipole orientation and impurity ions, respectively. Observing this behavior for DBAF suggests that the motion of anions and cations is correlated to the extent that the dielectric signature is analogous to dipoles, where the distance of opposite charges is fixed. A separate dc-conductivity signal at lower frequencies would then originate from a small percentage of ions which are relatively free to diffuse across longer distances. In terms of the modulus representation of Figure 7, the separation of dc- and ac-conductivity appears as two distinct peaks in the imaginary part $M''(\omega)$, where the low- and high-frequency peaks are respectively characterized by τ_σ and τ_M. Based on the faster peak (τ_M) relaxing the fraction of $\Delta M/M_\infty = \Delta M \times \epsilon_\infty = 0.29 \times 3.2 = 93\%$ of the electric field, τ_M instead of τ_σ will dominate the relaxation time of the electric field (at constant charge condition). Preliminary data for other systems confirm that the time scale of solvation dynamics in ionic liquids matches the relaxation time of the (macroscopic) electric field as characterized by the modulus $M = 1/\epsilon$. The concomitant time scale τ_M reflects the longitudinal dielectric time constant in the case of a continuum type dielectric subject to a homogeneous field.

4. Summary and Conclusions

We have characterized the dynamics of a supercooled ionic liquid, dibutylammonium formate, by solvation dynamics, probe rotation, and dielectric relaxation experiments. This study focuses on the viscous regime of the glass-forming ionic liquid, just above the glass transition temperature. On the basis of the solvation response amplitude $\Delta\nu = 300$ cm^{-1} for the probe quinoxaline and on the dielectric constant $\epsilon_s = 43$, this liquid is moderately dipolar on both the microscopic (solvation dynamics) as well as the macroscopic (dielectric relaxation) level. Although the time scales for solvation, probe rotation, and dielectric relaxation are all different, they follow a common Vogel−Fulcher−Tammann type temperature dependence with a glass transition near $T_g = 153$ K and a fragility index around $m = 70$. The rotational motion of the triplet-state probe quinoxaline follows the behavior expected on the basis of molecular liquids regarding the time constant and relaxation time dispersion relative to the dynamics of the solvent. Because the size of the probe is similar to those of the anions and cations, its dynamics is not exponential ($\beta_{rot} = 0.65$) and not slowed significantly ($\tau_{rot}/\tau_{sol} = 6$).

In terms of a Kohlrausch−Williams−Watts analysis, the Stokes-shift correlation function derived from solvation data is characterized by a stretching exponent as low as $\beta_{sol} = 0.4$, indicative of a highly nonexponential solvent response as found for other ionic liquids near or above room temperature. This contrasts the increase of β toward unity typical for molecular liquids of similar fragility, which occurs as the relaxation time is decreased from 100 s to below 1 ns. The solvation dynamics time scale τ_{sol} is considerably shorter than those of dielectric retardation τ_ϵ and dc-conductivity τ_σ and the dielectric loss peak is associated with a high value of the stretching exponent, $\beta_\epsilon = 0.8$. However, the true dielectric relaxation time τ_M of the electric modulus $M = 1/\epsilon$ coincides well with the observed solvent response regarding both time scale and KWW exponent β. We conclude that dipolar solvation in these ionic liquids is best represented by the relaxation behavior of the macroscopic electric field with respect to the average time constant τ and to the degree of relaxation time dispersion in terms of β. The inhomogeneous line width of the $T_1 \rightarrow S_0(0-0)$ emission does not show the signature of heterogeneous dynamics found in molecular liquids.

The dielectric loss curves of viscous dibutylammonium formate are more reminiscent of liquids consisting of molecular dipoles with some additional dc-conductivity that is well separated in frequency from the main asymmetrically broadened peak. This dielectric behavior is consistent with highly correlated anion/cation motion (long persistence time of ion pairs) and a small amount of ions with sufficient mobility to contribute to dc-conductivity on a time scale that is shifted considerably to lower frequencies. Other ionic systems tend to display a single loss or relaxation feature where ac- and dc-components are not clearly separable.

Acknowledgment. We thank C. A. Angell and his group for providing samples of ionic liquids. This material is based upon work supported by the National Science Foundation under Grant No. CHE 0204065.

Note Added after ASAP Publication. This article was published ASAP on February 11, 2006. Two entries in the first column of Table 3 have been modified. The correct version was posted on February 20, 2006.

References and Notes

(1) Rogers, R. D.; Seddon, K. R. *Science* **2003**, *302*, 792.
(2) Rogers, R. D.; Seddon, K. R., Eds. In *Ionic Liquids as Green Solvents*: *Progress and Prospects*; ACS Symp. Ser.; American Chemical Society: Washington, DC, 2003; No. 856.
(3) Rogers, R. D.; Seddon, K. R., Eds. In *Ionic Liquids IIIA*, *B*: *Fundamentals, Progress, Challenges, and Opportunities*; ACS Symp. Ser.; American Chemical Society: Washington, DC, 2005; Nos. 901 and 902.
(4) Wasserscheid, P.; Welton, T., Eds. In *Ionic Liquids in Synthesis*; Wiley-VCH: Weinheim, Germany, 2003.
(5) Wilkes, J. S. *Green Chem.* **2002**, *4*, 73.
(6) Wilkes, J. S. *J. Mol. Catal. A*: *Chem.* **2004**, *214*, 11.
(7) Giraud, G.; Gordon, C. M.; Dunkin, I. R.; Wynne, K. *J. Chem. Phys*. **2003**, *119*, 464.
(8) Cang, H.; Li, J.; Fayer, M. D. *J. Chem. Phys.* **2003**, *119*, 13017.
(9) Rajian, J. R.; Li, S. F.; Bartsch, R. A.; Quitevis, E. L. *Chem. Phys. Lett.* **2004**, *393*, 372.
(10) Shirota, H.; Funston, A. M.; Wishart, J. F.; Castner, E. W., Jr. *J. Chem. Phys.* **2005**, *122*, 184512.
(11) Dahl, K.; Sando, G. M.; Fox, D. M.; Sutto, T. E.; Owrutsky, J. C. *J. Chem. Phys.* **2005**, *123*, 084504.
(12) Noel, M. A. M.; Allendoerfer, R. D.; Osteryoung, R. A. *J. Phys. Chem.* **1992**, *96*, 2391.
(13) Kawai, A.; Hidemori, T.; Shibuya, K. *Chem. Lett.* **2004**, *33*, 1464.
(14) Evans, R. G.; Wain, A. J.; Hardacre, C.; Compton, R. G. *ChemPhysChem* **2005**, *6*, 1035.
(15) Noda, A.; Hayamizu, K.; Watanabe, M. *J. Phys. Chem. B* **2001**, *105*, 4603.
(16) Tokuda, H.; Hayamizu, K.; Ishii, K.; Abu Bin Hasan Susan, M.; Watanabe, M. *J. Phys. Chem. B* **2004**, *108*, 16593.
(17) Tokuda, H.; Hayamizu, K.; Ishii, K.; Susan, M. A. B. H.; Watanabe, M. *J. Phys. Chem. B* **2005**, *109*, 6103.
(18) Tsuzuki, S.; Tokuda, H.; Hayamizu, K.; Watanabe, M. *J. Phys. Chem. B* **2005**, *109*, 16474.
(19) Shim, Y.; Choi, M. Y.; Kim, H. J. *J. Chem. Phys.* **2004**, *122*, 044511.
(20) Kobrak, M. N.; Znamenskiy, V. *Chem. Phys. Lett.* **2004**, *395*, 127.
(21) Yan, T. Y.; Burnham, C. J.; Del Pópolo, M. G.; Voth, G. A. *J. Phys. Chem. B* **2004**, *108*, 11877.
(22) Lee, S. U.; Jung, J.; Han, Y. K. *Chem. Phys. Lett.* **2005**, *406*, 332.
(23) Margulis, C. J. *Mol. Phys.* **2004**, *102*, 829.
(24) Aki, S. N. V. K.; Brennecke, J. F.; Samanta, A. *Chem. Commun.* **2001**, 413.
(25) Anderson, J. L.; Ding, J.; Welton, T.; Armstrong, D. W. *J. Am. Chem. Soc.* **2002**, *124*, 14247.
(26) Ogihara, W.; Aoyama, T.; Ohno, H. *Chem. Lett.* **2004**, *33*, 1414.
(27) Reichardt, C. *Green Chem.* **2005**, *7*, 339.
(28) Maroncelli, M. *J. Mol. Liq.* **1993**, *57*, 1.
(29) Karmakar, R.; Samanta, A. *J. Phys. Chem. A* **2002**, *106*, 6670.
(30) Karmakar, R.; Samanta, A. *J. Phys. Chem. A* **2003**, *107*, 7340.
(31) Saha, S.; Mandal, P. K.; Samanta, A. *Phys. Chem. Chem. Phys.* **2004**, *6*, 3106.
(32) Baker, S. N.; Baker, G. A.; Bright, F. V. *Green Chem.* **2002**, *4*, 165.
(33) Baker, S. N.; Baker, G. A.; Munson, C. A.; Chen, F.; Bukowski, E. J.; Cartwright, A. N.; Bright, F. V. *Ind. Eng. Chem. Res.* **2003**, *42*, 6457.
(34) Ingram, J. A.; Moog, R. S.; Ito, N.; Biswas, R.; Maroncelli, M. *J. Phys. Chem. B* **2003**, *107*, 5926.
(35) Arzhantsev, S.; Ito, N.; Heitz, M.; Maroncelli, M. *Chem. Phys. Lett*. **2003**, *381*, 278.
(36) Ito, N.; Arzhantsev, S.; Heitz, M.; Maroncelli, M. *J. Phys. Chem. B* **2004**, *108*, 5771.
(37) Ito, N.; Arzhantsev, S.; Maroncelli, M. *Chem. Phys. Lett.* **2004**, *396*, 83.
(38) Arzhantsev, S.; Jin, H.; Ito, N.; Maroncelli, M. *Chem. Phys. Lett.* **2005**, *417*, 524.
(39) Chowdhury, P. K.; Halder, M.; Sanders, L.; Calhoun, T.; Anderson, J. L.; Armstrong, D. W.; Song, X.; Petrich, J. W. *J. Phys. Chem. B* **2004**, *108*, 10245.
(40) Bonhôte, P.; Dias, A. P.; Papageorgiou, N.; Kalyanasundaram, K.; Grätzel, M. *Inorg. Chem.* **1996**, *35*, 1168.
(41) MacFarlane, D. R.; Forsyth, S. A.; Golding, J.; Deacon, G. B. *Green Chem.* **2002**, *4*, 444.
(42) Holbrey, J. D.; Reichert, W. M.; Nieuwenhuyzen, M.; Johnston, S.; Seddon, K. R.; Rogers, R. D. *Chem. Commun.* **2003**, 1636.
(43) Berg, R. W.; Deetlefs, M.; Seddon, K. R.; Shim, I.; Thompson, J. M. *J. Phys. Chem. B* **2005**, *109*, 19018.
(44) Angell, C. A.; Ngai, K. L.; McKenna, G. B.; McMillan, P. F.; Martin, S. W. *J. Appl. Phys.* **2000**, *88*, 3113.
(45) Xu, W.; Cooper, E. I.; Angell, C. A. *J. Phys. Chem. B* **2003**, *107*, 6170.
(46) Xu, W.; Angell, C. A. *Science* **2003**, *302*, 422.
(47) Yoshizawa, M.; Xu, W.; Angell, C. A. *J. Am. Chem. Soc.* **2003**, *125*, 15411.
(48) Hirao, M.; Sugimoto, H.; Ohno, H. *J. Electrochem. Soc.* **2000**, *147*, 4168.
(49) Ohno, H.; Yoshizawa, M. *Solid State Ionics* **2002**, *154*, 303.
(50) Noda, A.; Susan, A. B.; Kudo, K.; Mitsushima, S.; Hayamizu, K.; Watanabe, M. *J. Phys. Chem. B* **2003**, *107*, 4024.
(51) Richert, R.; Stickel, F.; Fee, R. S.; Maroncelli, M. *Chem. Phys. Lett.* **1994**, *229*, 302.
(52) Richert, R. *J. Chem. Phys.* **2000**, *113*, 8404.
(53) Weingärtner, H.; Knocks, A.; Schrader, W.; Kaatze, U. *J. Phys. Chem. A* **2001**, *105*, 8646.
(54) Wakai, C.; Oleinikova, A.; Ott, M.; Weingärtner, H. *J. Phys. Chem. B* **2005**, *109*, 17028.
(55) Asaki, M. L. T.; Redondo, A.; Zawodzinski, T. A.; Taylor, A. J. *J. Chem. Phys.* **2002**, *116*, 10377.
(56) Rivera, R.; Brodin, A.; Rössler, E. A. *J. Non-Cryst. Solids.* Submitted for publication.
(57) Richert, R. *Rev. Sci. Instrum.* **1996**, *67*, 3217.
(58) Belieres, J.-P. Dissertation, Arizona State University, Tempe, 2005.
(59) Yang, M.; Richert, R. *Chem. Phys.* **2002**, *284*, 103.
(60) Wang, L.-M.; Richert, R. *J. Chem. Phys.* **2004**, *120*, 11082.
(61) Nickel, B.; Ruth, A. A. *J. Phys. Chem.* **1991**, *95*, 2027.
(62) Fee, R. S.; Maroncelli, M. *Chem. Phys.* **1994**, *183*, 235.
(63) Richert, R. *J. Chem. Phys.* **2001**, *114*, 7471.
(64) Yang, M.; Richert, R. *J. Chem. Phys.* **2001**, *115*, 2676.
(65) Richert, R.; Richert, M. *Phys. Rev. E* **1998**, *58*, 779.
(66) Matyushov, D. V. *J. Chem. Phys.* **2001**, *115*, 8933.
(67) Richert, R. *J. Phys.*: *Condens. Matter* **2002**, *14*, R703.
(68) Richert, R.; Wagener, A. *J. Phys. Chem.* **1991**, *95*, 10115.
(69) Wendt, H.; Richert, R. *J. Phys. Chem. A* **1998**, *102*, 5775.